Pseudo-rigid Body Modeling of IPMC for a Partially Compliant Four-bar Mechanism for Work Volume Generation

ARTICLE *in* JOURNAL OF INTELLIGENT MATERIAL SYSTEMS AND STRUCTURES · JANUARY 2009

Impact Factor: 2.07 · DOI: 10.1177/1045389X08088784

3 AUTHORS, INCLUDING:

Bishakh Bhattacharya
Indian Institute of Technology Kanpur
62 PUBLICATIONS **150** CITATIONS
SEE PROFILE

Ashish Dutta
Indian Institute of Technology Kanpur
56 PUBLICATIONS **163** CITATIONS
SEE PROFILE

Pseudo-rigid Body Modeling of IPMC for a Partially Compliant Four-bar Mechanism for Work Volume Generation

Dibakar Bandopadhya, Bishakh Bhattacharya and Ashish Dutta

Journal of Intelligent Material Systems and Structures 2009 20: 51 originally published online 11 July 2008
DOI: 10.1177/1045389X08088784

Pseudo-rigid Body Modeling of IPMC for a Partially Compliant Four-bar Mechanism for Work Volume Generation

DIBAKAR BANDOPADHYA,* BISHAKH BHATTACHARYA AND ASHISH DUTTA

Department of Mechanical Engineering, IIT Kanpur, Kanpur 208 016, India

ABSTRACT: Conventional four-bar crank rocker mechanisms made of rigid links can generate only one path, at the rocker tip, for one revolution of the crank. However, if the rocker length can be actively changed then its tip can generate a work volume. This study describes an application of ionic polymer metal composite (IPMC) as a partially compliant rocker in a four-bar mechanism for work volume generation. First, an experiment is conducted to study the voltage verses bending characteristics of IPMC and based on the experimental data the IPMC is modeled using a pseudo rigid body model. The model is based on the fix-pin support type of cantilever mode and its derivation is explained in detail. The maximum and minimum length of the rocker is controlled by changing the voltage applied to it and this generates a work volume for one revolution of the crank. Simulation results are compared with the experimentally obtained work volume and the differences are found. The proposed mechanism has the potential for application in micro positioning, compliant structures, etc.

Key Words: ionic polymer metal composite, four-bar mechanism, work volume, pseudo-rigid body model.

INTRODUCTION

FOUR-BAR mechanisms have traditionally been made of rigid links. In the case of a conventional crank rocker mechanism the rocker tip (or a coupler point) generates a single path for one revolution of the crank. In case the length of the rocker is varied, a work volume can be generated. Such adjustable four-bar mechanisms with an adjustable rocker have been made earlier using a prismatic joint in the rocker to vary its length (Hong and Erdman, 2005). However, such mechanisms are quite large in size and require high power due to the prismatic joint and actuators required to change the rocker length. In this study, the authors propose a small partially complaint four-bar mechanism with ionic polymer metal composite (IPMC) as an adjustable rocker. The IPMC being small in size, the overall length of the four-bar mechanism can be kept small. In addition, the actuation of the IPMC requires very low voltage and its control does not involve sophisticated controllers. Hence, it is ideal for micro-scale applications.

The objectives of this study are:

(a) Experimentally measure the deflection of an IPMC due to varying voltage inputs and, based on it, model the IPMC using pseudo-rigid body technique.
(b) Develop a four-bar mechanism with a compliant IPMC rocker in which the other links are rigid.
(c) Vary the length of the IPMC for one revolution of the crank and obtain a work volume.
(d) Compare the simulation and the experimental results.

Several types of compliant mechanism and their analysis using pseudo-rigid body model have been shown in Howell and Midha (1994) and Midha et al. (2000). Flying insect robots, where compliant four-bar mechanism has been used successfully for high degree of maneuverability (Shimoyama et al., 1993; Garcia and Goldfarb, 1998; Fearing et al., 2000; Yan et al., 2001) and compliant wing structure for micromechanical flying insect (MFI) robot (Sitti, 2001). A few of the varying path generation of closed loop linkages have been reported in Tao and Sadler (1995), Lin and Chen (1996), Tokuz and Uyan (1997) and Zhang et al. (1999). Saggere and Kota (2001) have developed a four-bar mechanism for segmented path generation with a flexible coupler which undergoes prescribed shape along with the rigid body motion.

The IPMC is a class of electro-active polymer (EAP) that is gaining importance as an actuator due to its large bending deflection with low actuation voltage. EAPs are divided into two groups: those driven by an electric field and those driven by the diffusion of ions. Details of the working of an IPMC is given in Shahinpoor et al. (1998), Bar-Cohen et al. (2002), Zeng et al. (2005) and

*Author to whom correspondence should be addressed.
E-mail: dibakarb@iitk.ac.in
Figures 2–4, 6 and 11–21 appear in color online: http://jim.sagepub.com

1045-389X/09/01 051–11 $10.00/0 DOI: 10.1177/1045389X08088784

Lee et al. (2007). Several aspects of the manufacture of IPMC have been described in Shahinpoor and Kim (2000, 2001, 2004, 2005) and Kim and Shahinpoor (2003). Applications of IPMC for vibration attenuation are given in Bandopadhya et al. (2007a,b).

The motion of the proposed four-bar mechanism is not in the gravity plane and hence the IPMC is not affected by gravitational forces. In addition, the IPMC does not transmit any torque as the input to the system is given to the crank by a DC motor. The rocker follows the motion of the crank via the coupler. As the crank is operated at very slow speeds the dynamic forces on the rocker are negligible. Hence the low load carrying capacity of the IPMC does not affect the functioning of the mechanism. The IPMC used is of size $40 \times 5 \times 1\,\text{mm}^3$. An experiment is conducted to study the relation between the deflection and the voltage applied to the IPMC in cantilever mode. Cantilever mode of one end fixed and other pin joint for the IPMC rocker has been analyzed using pseudo-rigid body modeling technique as proposed in Howell (2001). Simulations are performed using the pseudo-rigid body modeling technique and it is found that it matches with the circular bending model of IPMC as obtained from the experiments. Using these results a four-bar mechanism is designed with IPMC based rocker. Experimentally, it is shown that by applying a voltage source at the rocker end a work volume generation is possible. In the next section, IPMC has been studied experimentally to obtain its bending characteristics to obtain the bending moment–curvature and curvature–voltage relationship. The pseudo-rigid body modeling of the IPMC-rocker is then presented. The limit positions of the partially compliant four-bar mechanism have been discussed. The circular bending model of the IPMC-rocker for varying work volume generation is then discussed. The simulation results and comparative discussions are then presented while the section that follows deals with the experiment results. Finally, conclusions are drawn.

BENDING CHARACTERISTIC OF IPMC

An IPMC is kept in the cantilever mode with one end fixed and a controlled voltage is applied at the fixed end. The voltage is increased in steps and the corresponding deflections are recorded on a graph paper. The IPMC of size $40 \times 5 \times 1\,\text{mm}^3$, purchased from Environment Inc., Virginia, USA, is used and water is used as the polar solvent. The experiment is conducted in cantilever mode subjected to an input voltage up to 4.5 V to calibrate its bending characteristic. Copper strips are used at one end and voltage is applied quasi-statically from a DC power supply (0–60 V, 0–10 A). IPMC is bent under an input voltage up to 4.5 V starting from 0.5 V with an increment of 0.5 V in each step. For each input voltage after 30 s tip deflection of the IPMC has been recorded. The radius of curvature R for an input voltage V is obtained as $R = 1/\phi$, where, l is the length of the IPMC and ϕ is the tip angle of IPMC. From Figure 1, for an arbitrary tip position $P(u, v)$, $\tan\alpha = v/u$, further using Euler–Bernoulli equation of curvature one can get,

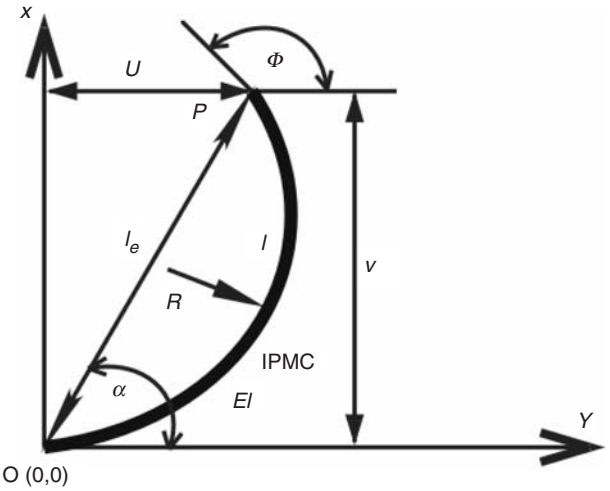

Figure 1. *Bending configuration of IPMC under applied voltage.*

$$\frac{d\phi}{ds} = \frac{M_b}{EI} \tag{1}$$

where, $d\phi/ds$ is the rate of change in angular deflection along the IPMC strip (curvature s), M_b is the bending moment generated due to input voltage V, and EI is the flexural rigidity of IPMC. From Equation (1) and on integration one can obtain the end point coordinates as:

$$u = W\sin\phi, \quad v = W(1-\cos\phi) \tag{2}$$

where, $W = EI/M_b$. Combining Equations (1) and (2) one gets,

$$\tan\alpha = \frac{W(1-\cos\phi)}{W\sin\phi} = \frac{1-\cos\phi}{\sin\phi} = \tan\frac{\phi}{2} \Rightarrow \phi = 2\alpha. \tag{3}$$

Experimentally α is known to us by locating tip position of the IPMC. Therefore, curvature–end tip angle relationship is obtained as:

$$\kappa = \frac{1}{R} = \frac{\phi}{l} = \frac{2\alpha}{l} \tag{4}$$

Figure 2 shows the change in radius of curvature with respect to the tip angle of the IPMC for each input voltage. The tip angle is obtained experimentally for every bending sequence of IPMC. This clearly demonstrates how the radius of curvature is varying even for

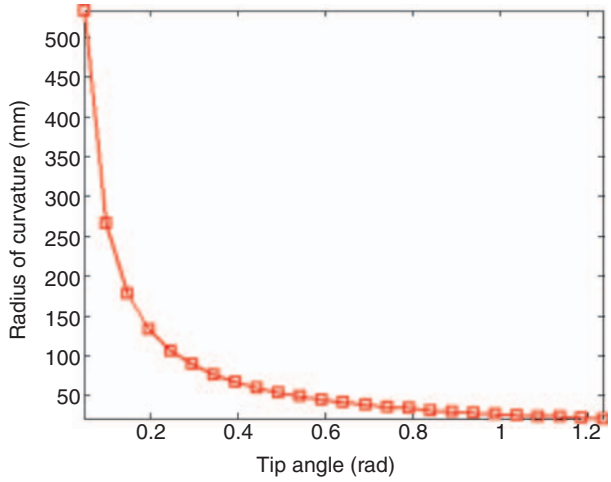

Figure 2. *Change in radius of curvature of bent IPMC with the change in tip angle.*

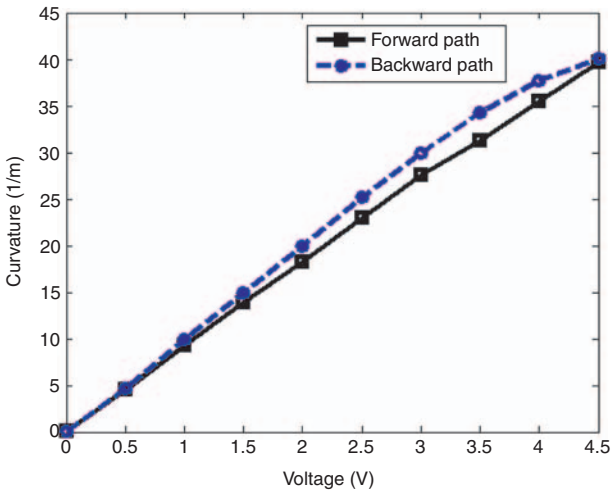

Figure 3. *Voltage–curvature relationship of IPMC obtained experimentally.*

a small variation of tip angle. Further, it is assumed that IPMC is bending with linearly varying curvature. In order to verify this assumption experimentally, tip angles of the IPMC have been obtained and subsequently curvature of IPMC is plotted for each input voltage. After measuring the end point deflection of IPMC for each input voltage, the relation given in Equation (4) is used to obtain the curvature–voltage relationship for both increasing and decreasing input voltage as plotted in Figure 3. The average curvature is then used to obtain the bending moment and input voltage relationship. The experiment clearly demonstrates the hysteresis losses it undergoes due to dehydration.

Therefore, from the experiment one can assume,

$$\kappa = \frac{1}{R} = k \times V \quad 0 \leq V \leq 5 \tag{5}$$

where, k is a path constant, which can be determined from the experimental data and V is the applied voltage. The value of k depends on the backbone materials, counter ions and its amount, and the property of the solvent present as given in (Shahinpoor et al., 1998). The bending moment generated due to the input voltage to IPMC rocker is given by

$$M_b = EI \times \kappa \tag{6}$$

where, E is the modulus of elasticity of IPMC and I is the area moment of inertia. Bending moment generated completely depends on the moisture content and subsequently movement of ions within IPMC and the backbone materials. Hence, the electrode properties do not affect the generated moment and also the thickness of the electrode is very small so it does not affect the elastic modulus of the base polymer material. The IPMC used in the experiment is thick (1 mm) and can withstand a large potential of around 5 V for a short time. However, dehydration due to moisture loss through the porous metal electrode on the polymer surface affects the repeatability of the IPMC. Each cycle of the four-bar motion is carried out in about 10 s and hence the IPMC does not get enough time to back relax in this short time.

PSEUDO-RIGID BODY MODELING OF IPMC-ROCKER

The experimental results obtained in the previous section are used to model the bending characteristics of the IPMC using a pseudo rigid body model (Howell, 2001). The maximum bending moment generated for each input voltage is given as ($M_b = EI \times \kappa$), where, κ is the average curvature obtained experimentally for each input voltage, which includes all the distributed pressure effects. An analogy has been drawn that the bending phenomena is equivalent to the same amount of tip deflection that is caused by an external bending moment M_b acting at the tip of IPMC. This concept is employed here to model the IPMC for each bending moment obtained for each input voltage. The pseudo-rigid body modeling technique has been followed considering end-moment at the rocker point, to obtain the end-point deflection of IPMC-rocker in cantilever mode of one end fixed and other pin joint. Voltage is applied at one end and subsequently end point deflection has been obtained. Bending moment and the deflection angle are related as ($M_b = K_s\Theta$) where, Θ is the corresponding pseudo-rigid body angle and K_s is the spring constant. Figure 4 shows the equivalent bending model in cantilever mode for an input voltage V. The main objective is to find out the spring constant and pseudo-rigid body angle of the IPMC.

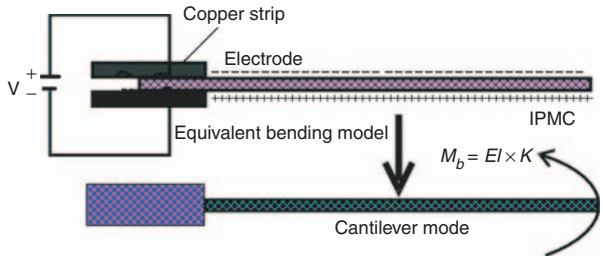

Figure 4. *Equivalent bending model of IPMC for input voltage V.*

Using the curvature–moment relationship one can obtain:

$$\frac{d\theta}{ds} = \frac{M_b}{EI} \tag{7}$$

where, θ is the tip angle of the rocker. Both the tip angles, ϕ (Equation (1)) and θ are equivalent to each other. For small length of flexural pivot one can assume that $\Theta = \theta$, and then spring constant is obtained as:

$$K_s = \frac{EI}{l_3} \tag{8}$$

where, l_3 is the length of the IPMC-rocker. During motion of the four-bar mechanism, a tangential force will act at the tip of the rocker, this will produce a resultant bending moment at the rocker. Considering resultant bending moment acting at the rocker is M_t then:

$$M_t = K_t \Theta. \tag{9}$$

This moment can also be expressed in terms of the resultant transverse force F_t multiplied by the moment arm (the length of the pseudo-rigid link), thus one can write, $M_t = F_t \gamma l_3$ where, γ is the characteristic radius factor. Combining with Equation (9) $F_t = K_t \Theta / \gamma l_3$, introducing force–deflection relationships in terms of the nondimensionalized load term (Howell, 2001).

$$(\alpha_t^2) = \frac{F_t l_3^2}{EI}. \tag{10}$$

The spring constant is directly obtained as:

$$K_t = \gamma K_\theta \frac{EI}{l_3} = 1.5164 \times \frac{EI}{l_3} \tag{11}$$

where, characteristic radius factor $\gamma = 0.7346$ and stiffness coefficient $K_\theta = 2.07$ (Howell, 2001).

Pseudo-rigid Body Modeling of Fixed-pinned IPMC-rocker

The pseudo-rigid body model of the IPMC-rocker is shown in Figure 5. Here, the rocker is replaced by a link

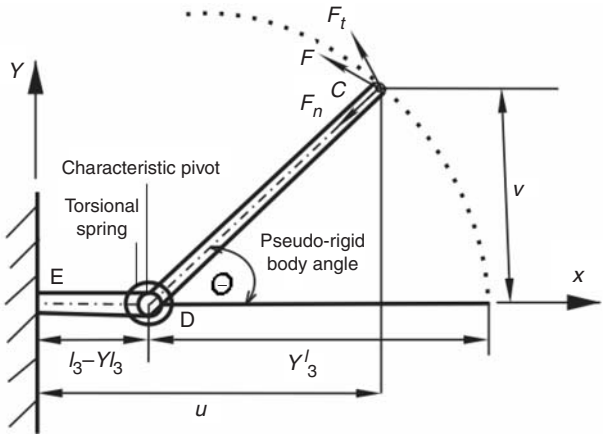

Figure 5. *Pseudo-rigid body modeling of rocker made of IPMC.*

with a characteristic pivot located at a length γl_3 from the free end of the rocker. It is assumed that a circular path can be accurately modeled by two rigid links that are connected at a pivot along the IPMC strip. A torsional spring at the pivot represents the IPMC strip's resistance to deflection. The location of this pseudo-rigid-body characteristic pivot is measured from the IPMC tip end as a fraction of the IPMC length, where the fractional distance is γl and γ is the characteristic radius factor. The product γl, the characteristic radius, is the radius of the circular deflection path traversed by the end of the pseudo-rigid body link. It is also the length of the pseudo-rigid body link.

Now, from Figure 5 one can obtain end point coordinates of the link as:

$$\begin{aligned} v &= \gamma l_3 \sin\theta, u = (l_3 - \gamma l_3) + \gamma l_3 \cos\theta \\ &= l_3 - \gamma l_3(1 - \cos\theta) = l_3\{1 - \gamma(1 - \cos\theta)\} \end{aligned} \tag{12}$$

where, ED denotes the length of characteristic pivot located from the fixed end, DC denotes the pseudo-rigid body length, and EC is the effective length. Therefore, effective length of the rocker is found out as:

$$l_{3e} = l_3\sqrt{1 + 2\gamma(1 - \cos\theta)(\gamma - 1)} \tag{13}$$

Figure 6 shows the change in tip position of the IPMC-rocker for different input voltages.

Force using Free Body Diagram

The free body diagram of the mechanism is shown in Figure 7. For the links to be in static equilibrium the following conditions must be satisfied:

$$\sum F_x = 0 \quad \sum F_y = 0 \quad \sum M = 0.$$

The reaction forces on each link are labeled as F_{ij} i.e., the subscripts indicate the link number. The equations of equilibrium may be written for link 1 as

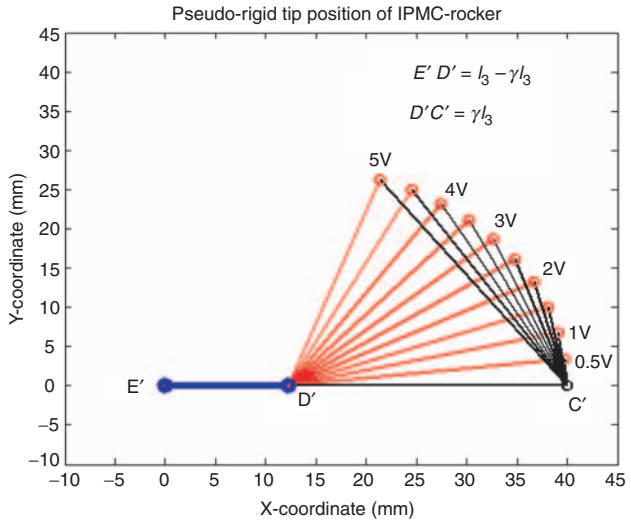

Figure 6. *Change in tip position of the IPMC-rocker following the pseudo-rigid body modeling, voltage ranges from 0.5 to 5 V.*

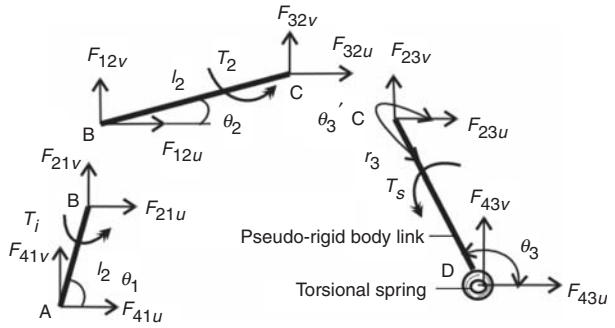

Figure 7. *Free body diagrams for the three moving links of the four-bar mechanism.*

(where considering u, v are the variables along x, y direction, respectively):

$$F_{41u} + F_{21u} = 0, F_{41v} + F_{21v} = 0.$$

Taking the moment about point 'A' one gets

$$T_i + F_{21v} l_1 \cos\theta_1 - F_{21u} l_1 \sin\theta_1 = 0 \tag{14}$$

Similarly for link 2,

$$F_{12u} + F_{32u} = 0, F_{12v} + F_{32v} = 0,$$

Taking moment about B

$$T_2 + F_{32v} l_2 \cos\theta_2 - F_{32u} l_2 \sin\theta_2 = 0 \tag{15}$$

And finally for link 3,

$$F_{43u} + F_{23u} = 0, F_{43v} + F_{23v} = 0,$$

Taking moment about point C one has

$$T_s + F_{43v} r_3 \cos\theta_3' - F_{43u} r_3 \sin\theta_3' = 0 \tag{16}$$

Considering $F_{41u} = a$, then $F_{21u} = -a$, $F_{12u} = a$ and $F_{32u} = -a = F_{23u}$ (joint C is fixed), $F_{43u} = a$ similarly

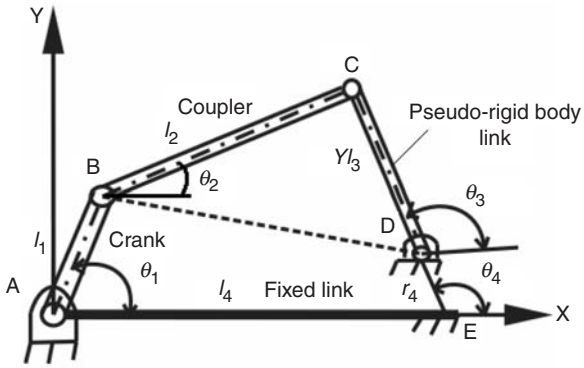

Figure 8. *Pseudo-rigid body modeling is applied to four-bar mechanism.*

$F_{41v} = b$, then $F_{21v} = -b$, $F_{12v} = b$ and $F_{32v} = -b = F_{23v}$, $F_{43v} = b$, solving Equations (14) and (16) one gets

$$a = F_{td} = \frac{T_i r_3 \cos\theta_3 + T_s l_1 \cos\theta_1}{l_1 r_3 \sin(\theta_3 + \theta_1)} \tag{17}$$

where, F_{td} is a tangential force. Similarly,

$$b = \frac{T_i r_3 \sin\theta_3 + T_s l_1 \sin\theta_1}{l_1 r_3 \sin(\theta_3 + \theta_1)} \tag{18}$$

Therefore, bending moment generated is found out as:

$$\begin{aligned} M_{\mathrm{d}} &= F_{td} \times \gamma l_3 \sin\theta_3 \\ &= \frac{T_i r_3 \cos\theta_3 + T_s l_1 \cos\theta_1}{l_1 r_3 \sin(\theta_3 + \theta_1)} \times r_3 \sin\theta_3 \end{aligned} \tag{19}$$

where, ($\theta_3' = \theta_3 + \pi$), r_3 is the length of the pseudo-rigid body link that is given by $r_3 = \gamma l_3$, T_{s} is the torque produced by the torsional spring and is given by:

$$T_{\mathrm{s}} = \gamma K_\theta \frac{E_p I}{l_3} \times (\theta_3 - \theta_{3,0}) \tag{20}$$

where, $\theta_{3,0}$ is the angle of the undeformed IPMC. The four-bar mechanism with compliant IPMC-rocker is modeled using pseudo rigid body method as shown in Figure 8. The pseudo-rigid body links (CD) are given by γl_3 and length (DE) given by $r_4 = l_3 - \gamma l_3$.

The coordinates of the point C is obtained as:

$$\begin{aligned} x_c &= l_4 + l_{3e} \cos\theta_3 \\ y_c &= l_{3e} \sin\theta_3 \end{aligned} \tag{21}$$

where, θ_3 is the IPMC-rocker angle during rotation. The end point tip position calculations are obtained by using standard rigid body mechanism analysis.

LIMIT POSITIONS OF THE PARTIALLY COMPLIANT FOUR-BAR MECHANISM

A four-bar mechanism reaches its limit positions for one complete revolution of the crank i.e., angle θ_3 reaches its maximum and minimum position. Norton et al. (1994) have introduced the triangle inequality concept to study the inequality concept for a non-Grashofian four-bar mechanism based on their mobility. Ting (1989) has modified the triangle inequality concept and introduced the theorem of assemblability and revolvability pertaining to the four-bar mechanism. The triangular properties was used to find out the limit condition of the four-bar mechanism. The limit position of the mechanism depends on the range of the angle α as shown in Figure 9.

Limit Positions of the Rocker

Limit position of the rocker is obtained when θ_3 reaches its minimum value i.e., $\theta_3 = \theta_3^{\min}$ and when it reaches maximum i.e., $\theta_3^{\max} = \theta_3^{\min} + \alpha$. From Figure 9 one can obtain

$$\beta = \cos^{-1}\left\{\frac{l_4^2 + l_3^2 - l_2^2}{2l_4 l_3}\right\} \tag{22}$$

$$\alpha = \cos^{-1}\left\{\frac{l_4^2 + l_3^2 - (l_1 + l_2)^2}{2l_4 l_3}\right\} - \beta \tag{23}$$

Therefore, limit position is obtained as:

$$\theta_3^{\min} = 180^\circ - (\alpha + \beta), \theta_3^{\max} = 180^\circ - \beta \tag{24}$$

For the partially compliant rocker, limit position is obtained similarly as:

$$\theta_{3e}^{\min} = 180^\circ - (\alpha_e + \beta_e), \theta_{3e}^{\max} = 180^\circ - \beta_e \tag{25}$$

where, α_e, β_e are the angles corresponding to the effective length l_{3e} of the rocker. For link lengths $l_1 = 15\,\text{mm}$, $l_2 = 40\,\text{mm}$, $l_3 = 40\,\text{mm}$, $l_4 = 40\,\text{mm}$ limit position of the rocker is obtained as $\theta_3^{\min} = 93.12^\circ$ and $\theta_3^{\max} = 120^\circ$. Length of the path generated by the rocker tip is obtained as $s = l_3\ \alpha = 18.75\,\text{mm}$. A partially compliant rocker can have different limit positions according to its effective length.

Limit Angle Positions of the Crank

Limit position of the crank is obtained similarly when θ_1 reached its minimum value i.e., $\theta_1 = \theta_1^{\min}$ and when it reaches maximum i.e., $\theta_1^{\max} = 180^o + \theta_1^{\min} + \gamma$. Thus from Figure 9,

$$\theta_1^{\min} = \cos^{-1}\left\{\frac{(l_1 + l_2)^2 + l_4^2 - l_3^2}{2(l_1 + l_2)l_4}\right\} \tag{26}$$

$$\theta_1^{\min} + \gamma = \cos^{-1}\left\{\frac{l_2^2 + l_4^2 - l_3^2}{2l_2 l_4}\right\} \tag{27}$$

Therefore, limit position of the crank is obtained for the link lengths specified above as $\theta_1^{\min} = 46.6^o$ and $\theta_1^{\max} = 240^o$. Limit position of the crank is also varied according to the effective length of the compliant IPMC-rocker.

CIRCULAR BENDING MODEL OF THE IPMC-ROCKER

Circular bending model has been used to validate the proposed pseudo-rigid body model. The effective length of the IPMC-rocker is obtained through free body diagram as shown in Figure 10 and comparison is made subsequently with the proposed model for tip positioning.

In the figure, $OF = OG = R$ is the radius of curvature, FG is the effective length of IPMC of length l_3 and is denoted by l_{3e}, O is the center of the curvature and ϕ is the angle between the radii of curvature meeting two end

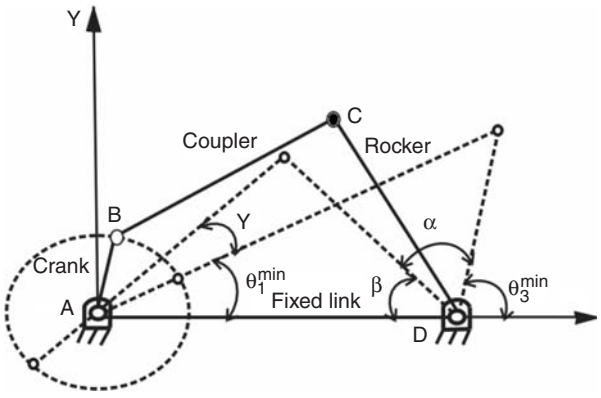

Figure 9. *Limit positions of a four-bar mechanism.*

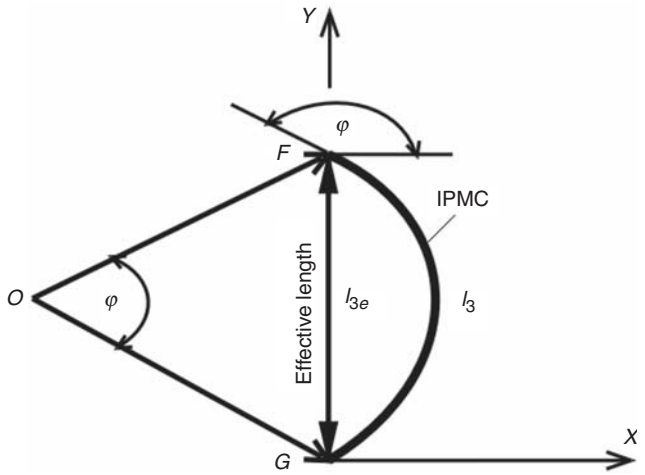

Figure 10. *Free body diagram of the bent IPMC-rocker.*

points of IPMC i.e., $\langle FOG = \phi$. The relation can be found as:

$$l_3 = R\phi \Rightarrow \phi = \frac{l_3}{R} \tag{28}$$

Therefore, ϕ can be calculated for a known bending configuration of IPMC. Using triangular properties, from triangle OFG one can get:

$$\cos\phi = \frac{OF^2 + OG^2 - FG^2}{2OF.OG} \tag{29}$$

Thus, effective length is obtained as:

$$l_{3e} = R\sqrt{2(1-\cos\phi)} \tag{30}$$

Figure 11 shows the circular bending pattern of IPMC for maximum input voltage of 5 V starting with initial input of 0.25 V.

SIMULATION RESULTS AND DISCUSSION

This section describes the generation of work volume by changing the effective length of the IPMC rocker. A program has been developed in MATLAB for path generation taking into account of the compliance of IPMC and the properties listed in Table 1. Coordinates of the points P_1, P_2, P_3 and P_4 are given in terms of link length and variable angle. Considering point P_1 at the origin, the coordinates of the other points are given by:

$$P_4(x_4 = l_4, y_4 = 0),$$
$$P_2(x_2 = l_1\cos\theta_1, y_2 = l_1\sin\theta_1)$$
$$P_3(x_3 = l_4 + l_{3e}\cos\theta_3, y_3 = l_{3e}\sin\theta_3).$$

A motor torque of 10 N mm at the crank is used for the simulation.

Figure 12 shows the tip position of the IPMC-rocker (AB) after application of input voltages. The results show that pseudo-rigid body modeling matched with the circular bending model of IPMC. Figure 13 shows the decrement of effective length for maximum input voltage of 5 V. Figure 14 shows the work volume generated for an input voltage of 5 V. It is found that increment of IPMC-rocker length, increases the work volume of the four-bar mechanism. Figure 15 shows the work volume (a–b–c–d–a) generated by the variable length rocker for an input voltage of 5 V following the circular bending model of IPMC. It is observed that the two work volumes generated are the same, although two different modeling techniques for IPMC are used.

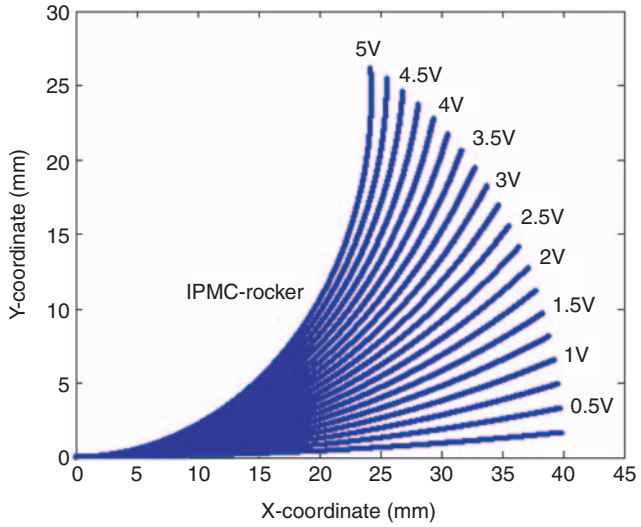

Figure 11. *Exact bending pattern of the IPMC- rocker for maximum input voltage of 5 V with increment of 0.25 V.*

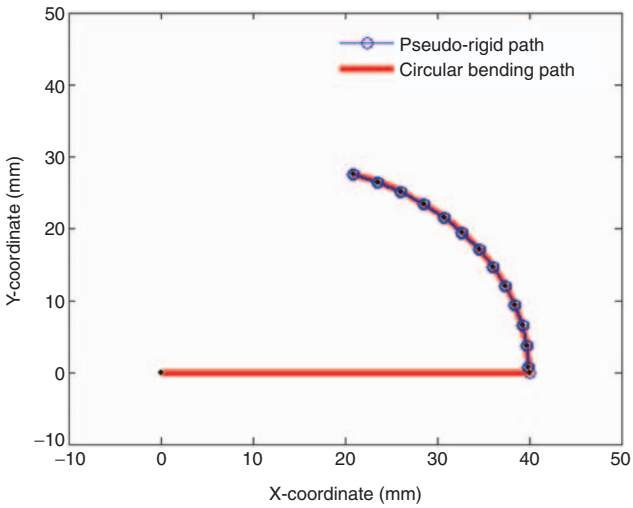

Figure 12. *Path followed by IPMC both for pseudo-rigid body analysis and circular bending model for an input of 5 V.*

Table 1. Four bar crank-rocker mechanism properties.

Crank length (l_1) = 15 mm	Width of IPMC (w) = 10 mm	Spring constant K_t = 37.91 N mm
Coupler length (l_2) = 40 mm	Thickness of IPMC (h) = 1 mm	Total time (t) = 10 s
Rocker length (l_3) = 40 mm	Modulus of elasticity (E) = 1.2 GPa	No of steps (n) = 500
Fixed length (l_4) = 40 mm	increment (θ_1) = 0.0126 rad	Maximum voltage input = 5 V

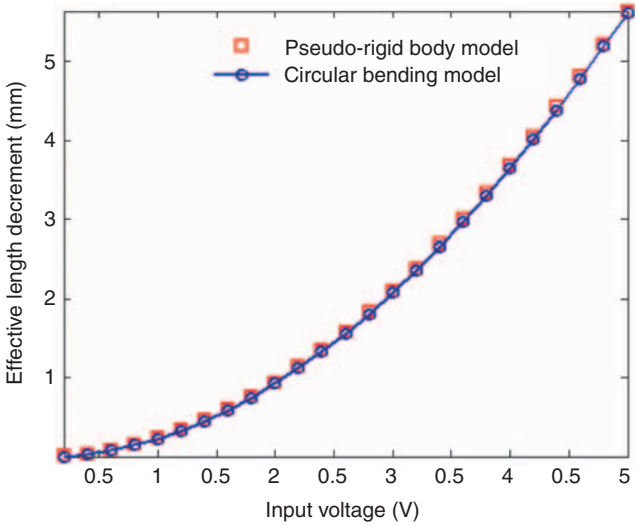

Figure 13. *Decrement of effective rocker length for maximum input voltages of 5 V for both pseudo-rigid body modeling and circular bending model.*

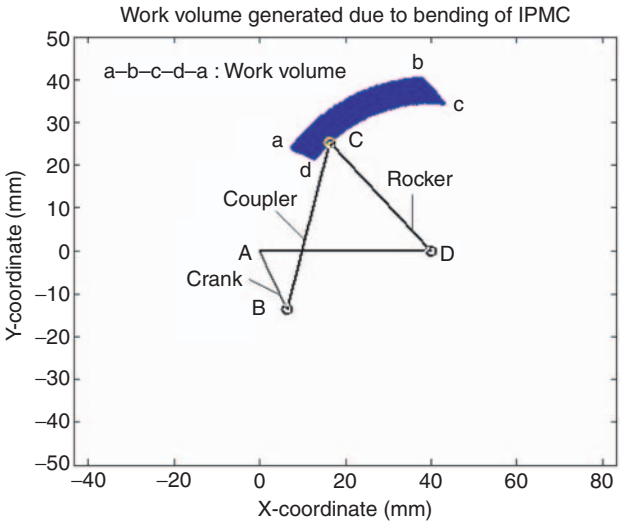

Figure 15. *Work volume generated following circular bending model of the IPMC-rocker for an input of 5 V.*

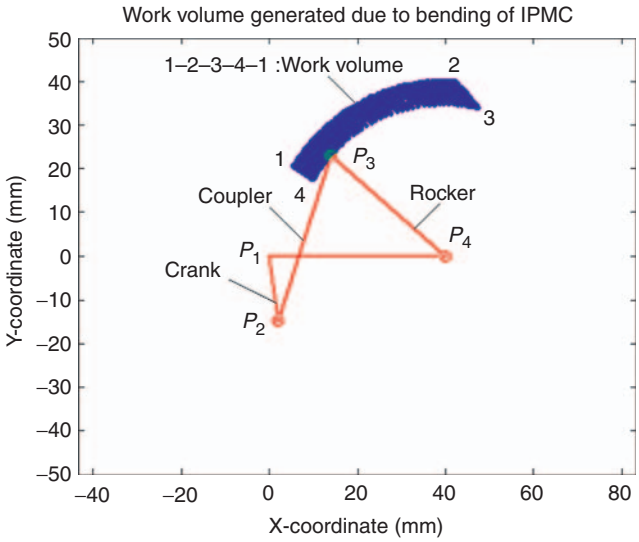

Figure 14. *Work volume generated by variable length rocker for an input voltage of 5 V following pseudo-rigid body modeling.*

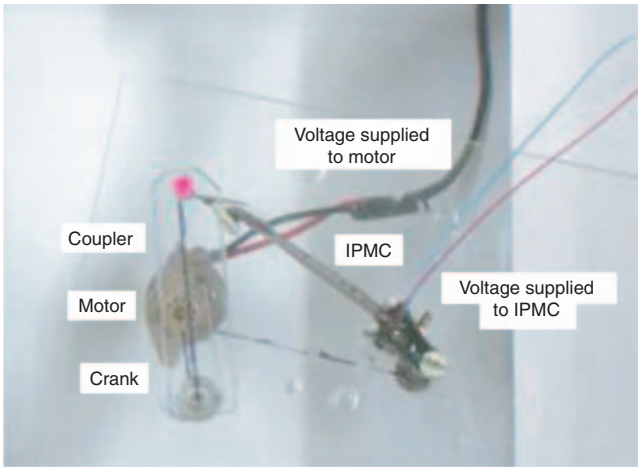

Figure 16. *Rocker is bending due to input voltage during motion of the four-bar mechanism.*

EXPERIMENT RESULTS AND DISCUSSION

An experimental setup of a partially compliant four-bar mechanism is designed as shown in Figure 16, with IPMC-rocker. The links are made of lightweight plastic and a DC motor (made by KTA Japan) is used to provide input torque to the crank. Crank and coupler form revolute joints, while one end of the IPMC link is fixed with a coupler and the other end with a revolute joint with the fixed link. Thus pseudo-rigid body modeling of rocker of fixed-pin support has been evaluated for work volume generation to compare with the theoretical results. The length of the crank is 15 mm while the coupler and fixed frame are each of 40 mm length. The size of the IPMC strip is $40 \times 5 \times 1\,\text{mm}^3$ and a set of two electrodes are placed at the joint end of the IPMC. The experiment is conducted to generate a single path for one complete revolution of crank in 10 s. The necessary control input and controller are shown in Figure 17.

In the experiment, the motion of the four-bar is recorded by a camera and the frames are processed to obtain the coordinates of the rocker tip. Figure 18 shows the comparison of the theoretical and experimental results for generating a single path. Figure 19 shows the variation of effective length of the rocker obtained from the experiment and the model. Figure 19 shows both the theoretical and experimental variation of effective length of the rocker. It is observed that the change in theoretical effective length is more compared to the experimental, as the change in effective length is affected due to dehydration, as time progresses.

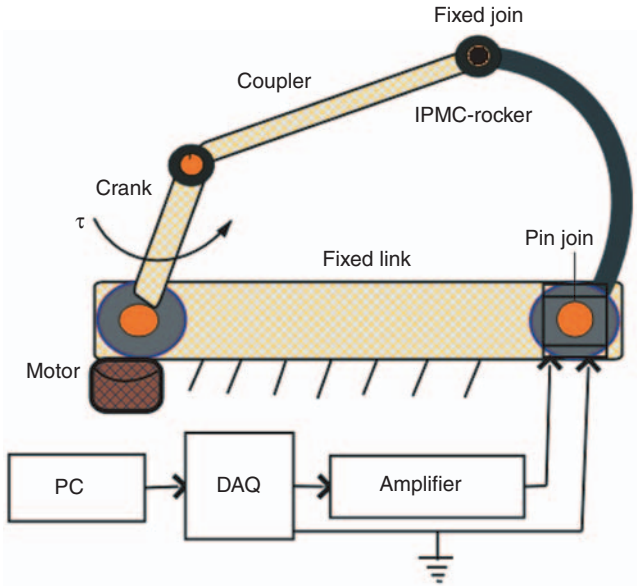

Figure 17. *Schematic diagram of the four-bar mechanism with the control strategy.*

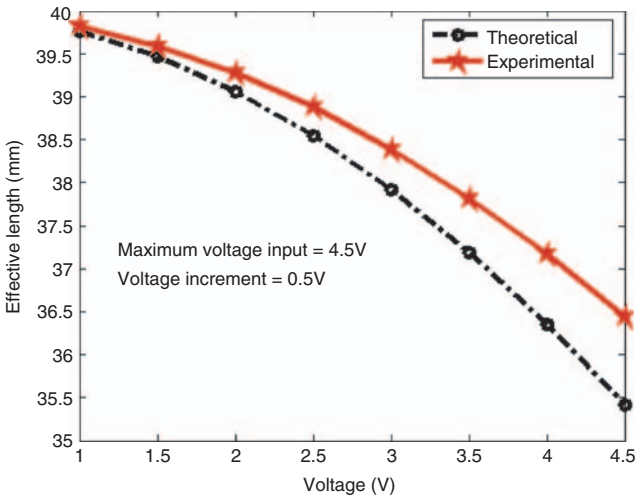

Figure 19. *Variation of effective length obtained experimentally and theoretically (pseudo-rigid body) for a maximum voltage input of 4.5 V with an increment of 0.5 V starting from 1 V.*

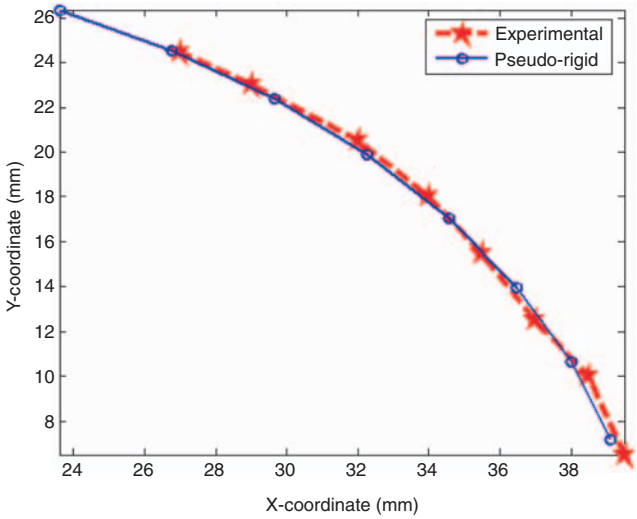

Figure 18. *Comparative study on rocker tip position experimentally and theoretically (pseudo-rigid body) for an input of 4.5 V with an increment of 0.5 V starting from 1 V.*

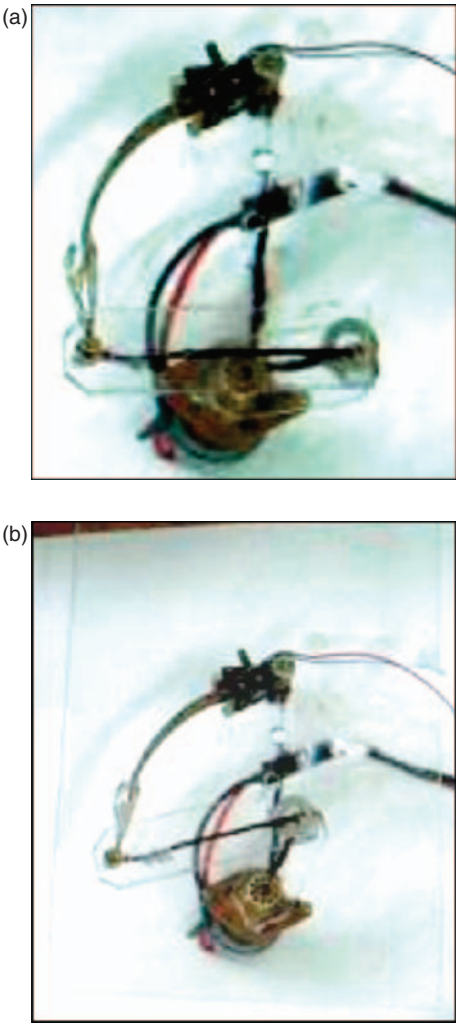

Figure 20. *(a) and (b) shows the end position of the bending motion of the IPMC-Rocker during work volume generation.*

Moreover, misalignment and bending resistance at the rocker point also affect effective length.

After comparing the paths generated by the rocker tip position, next the lengths of the IPMC is varied from maximum to minimum for one revolution of the crank. Figure 20 shows the two instantaneous IPMC-rocker end positions during the motion of the four-bar mechanism. Figure 21 shows the corresponding work volume for a maximum input voltage of 3 V and a minimum of 0 V. The outer curve is obtained by maintaining the IPMC at 0 V and then near the end of the curve (on the left side) the voltage is reduced to 3 V so that the rocker length is reduced. This generates the work volume. It is observed that the theoretically

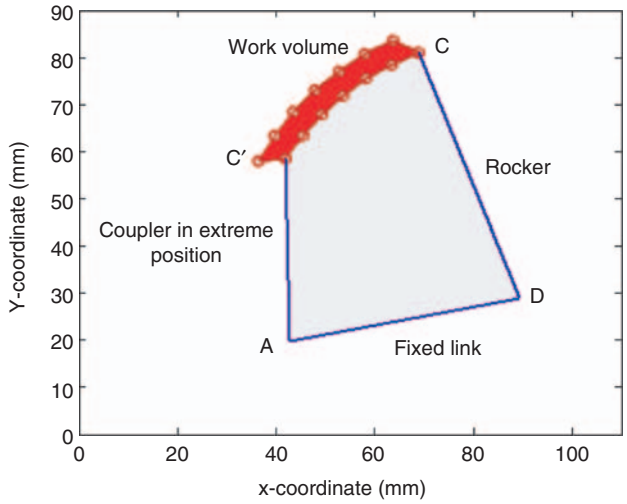

Figure 21. *Experimentally obtained work volume for a maximum input voltage of 3 V and a minimum voltage of 0 V.*

obtained work volume (shown in Figures 14 and 15) is larger as compared to the experimental one as higher change in effective length is recorded as shown in Figure 19. It is observed that after each revolution of the four-bar in 10 s the IPMC undergoes dehydration which affects the bending of IPMC for the next revolution. In addition, there may be some degree of misfit and misalignment at the joint connecting the rocker and the coupler which may affect the bending of the IPMC during rotation of the crank. These two parameters will cause some errors in the theoretically and experimentally obtained results.

CONCLUSIONS

This study presents a partially compliant four-bar mechanism for work volume generation in which the traditional rigid-body rocker has been replaced by an IPMC. Pseudo-rigid body modeling technique has been followed to model the rocker for variable path generation. It is proved theoretically and experimentally that pseudo-rigid body modeling technique gives precise results. This was also verified with the circular bending model of IPMC-rocker. This mechanism has the potential for application in micro-robotics and also in compliant mechanisms.

APPENDIX

Equation (7), integrating throughout rocker length one can obtain,

$$\int_0^{\theta} d\theta = \frac{M_b}{EI}\int_0^{l_3} ds \Rightarrow \theta = \frac{M_b l_3}{EI},$$

for small length flexural pivot one can assume, pseudo-rigid body angle Θ is equal to the tip angle θ of IPMC. Therefore, $M_b = K_s\Theta = \frac{EI}{l_3}\Theta$.

Equation (13) is obtained as:

$$l_{3e} = \sqrt{u^2+v^2} = \sqrt{l_3^2\{1-\gamma(1-\cos\theta)\}^2+(\gamma l_3\sin\theta)^2}$$

$$= l_3\sqrt{\{1-\gamma(1-\cos\theta)\}^2+\gamma^2\sin^2\theta}$$

$$= l_3\sqrt{1-2\gamma(1-\cos\theta)+\gamma^2(1-2\cos\theta+\cos^2\theta)+\gamma^2\sin^2\theta}$$

$$= l_3\sqrt{1-2\gamma(1-\cos\theta)+2\gamma^2(1-\cos\theta)}$$

Equation (17) is obtained as

$$a = \frac{T_i r_3\cos\theta_3' - T_s l_1\cos\theta_1}{l_1 r_3\sin(\theta_3'+\theta_1)} = \frac{T_i r_3\cos\theta_3 + T_s l_1\cos\theta_1}{l_1 r_3\sin(\theta_3+\theta_1)}.$$

REFERENCES

Bar-Cohen, Y., Bao, X., Sherrit, S. and Lih, S.S. 2002. "Characterization of the Electrochemical Properties of Ionic Polymer-Metal Composite (IPMC)," In: *Proceedings, SPIE Smart Structures and Materials Symposium, EAPAD Conference*, (page no) San Diego, CA, March 18–21.

Bandopadhya, D., Bhattacharya, B. and Dutta, A. 2007a. "An Active Vibration Control Strategy for a Flexible Link Using Distributed Ionic Polymer Metal Composites," *Smart Materials and Structures*, 16(3):617–625.

Bandopadhya, D., Bhattacharya, B., Dutta, A. 2007b. "Active Vibration Control Strategy for a Single Link Flexible Manipulator using Ionic Polymer Metal Composites," *Journal of Intelligent Material Systems and Structures*, 19(4):487–496.

Fearing, R., Chiang, K., Dickinson, M., Pick, D., Sitti, M. and Yan, J. 2000. "Transmission Mechanism for a Micromechanical Flying Insect," In: *Proceedings of the IEEE International Conference on Robotics and Automation*, pp. 1509–1516, San Francisco, CA USA, Apr.

Garcia, C.E. and Goldfarb, M.M. 1998. "Actuator Development for a Flapping Microrobotic Microaerial Vehicle," In: *SPIE Microrobotics Symposium*, Nov., Boston, USA.

Hong, B. and Erdman, A.G. 2005. "A Method for Adjustable Planer and Spherical Four Abr (Bar) Linkage Synthesis," *ASME Journal of Mechanism (Mechanical) Design*, 127(3):456–463.

Howell, L.L. 2001. *Compliant Mechanisms*, Wiley-Interscience.

Howell, L.L. and Midha, A. 1994. "A Method for the Design of Compliant Mechanisms with Small-length Flexural Pivots," *Journal of Mechanical Design*, 116(1):280–290.

Kim, K.J. and Shahinpoor, M. 2003. "Ionic Polymer Metal Composites–II Manufacturing Technique," *Smart Materials and Structure*, 12(1):65–69.

Lee, D.Y., Park, S., Lee, M.H., Kwang, J.K. and Heo, S. 2007. "Ionic Polymer-metal Composite Bending Actuator Loaded with Multi-walled Carbon Nanotubes," *Sensors and Actuators*, 133(1):117–127.

Lin, M.C. and Chen, J.S. 1996. "Experiments toward MRAC Design for Linkage System," *Mechatron*, 6(8):933–953.

Midha, A., Howell, L.L. and Tony, W.N. 2000. "Limit Positions of Compliant Mechanisms using the Pseudo-rigid-body Model Concept," *Mechanism and Machine Theory*, 35(1):99–115.

Norton, T.W., Howell, L.L. and Midha, A. 1994. "Graphical Synthesis for Limit Positions of a Four-bar Mechanism using the Triangle Inequality Concept," *Journal of Mechanical Design*, 116(4):1132–1140.

Sitti, M. 2001. "PZT Actuated Four-Bar Mechanism with Two Flexible Links for Micromechanical Flying Insect Thorax," In: *Proceedings of the IEEE, International Conference on Robotics and Automation*, (page no) Seoul, Korea, May 21–26.

Saggere, L. and Kota, S. 2001. "Synthesis of Planer, Compliant Four Bar Mechanisms for Compliant Segment Motion Generation," *ASME Journal of Mechanical Design*, 123(4):535–541.

Shahinpoor, M. and Kim, K.J. 2000. "The Effect of Surface Electrode Resistance on the Performance of Ionic-polymer Metal Composite (IPMC) Artificial Muscles," *Smart Materials and Structures*, 9(4):543–551.

Shahinpoor, M. and Kim, K.J. 2001. "Ionic Polymer Metal Composites Fundamentals I," *Smart Materials and Structures*, 10(4):819–833.

Shahinpoor, M. and Kim, K.J. 2004. "Ionic Polymer-metal Composites: III. Modeling and Simulation as Biomimetic Sensors, Actuators, Transducers, and Artificial Muscles," *Smart Materials and Structures*, 13(6):1362–1388.

Shahinpoor, M. and Kim, K.J. 2005. "Ionic Polymer-metal Composites: IV. Industrial and Medical Applications," *Smart Materials and Structures*, 14(1):197–214.

Shahinpoor, M., Bar-Cohen, Y., Simpson, J.O. and Smith, J. 1998. "Ionic Polymer-Metal Composites (IPMC) as Biomimetic Sensors, Actuators & Artificial Muscles – A Review," *Smart Materials and Structures*, 7(6):15–30.

Shimoyama, M.H., Suzuki, K. and Ezura, Y. 1993. "Insect-like Microrobots with External Skeletons," *IEEE Control Systems Magazine*, 13(1):37–41.

Tao, J. and Sadler, J.P. 1995. "Constant Speed Control of a Motor Driven Mechanism System," *Mechanism and Machine Theory*, 30(5):737–748.

Ting, K.L. 1989. "Mobility Criteria of Single-loop *N*-bar Linkages," *Journal of Mechanisms, Transmissions, and Automation in Design*, *Trans. ASME*, 111(4):504–507.

Tokuz, L.C. and Uyan, S. 1997. "Modeling, Simulation and Control of a Four-bar Mechanism with a Brushless Servo Motor," *Mechatron*, 7(4):369–383.

Yan, J., Wood, R., Avandhanula, S., Sitti, M. and Fearing, R. 2001. "Towards Flapping Wing Control for Micromechanical Flying Insect," In: *Proceeding of the IEEE International Conference on Robotics and Automation*, Korea.

Zhang, W.J., Li, Q. and Guo, L.S. 1999. "Integrated Design of Mechanical Structure and Control Algorithm for a Programmable Four-Bar Linkage," *IEEE, ASME Tran., on Mechatronics*, December, 4(4).

Zeng, C., Xiabo, T. and Shahinpoor, M. 2005. "Quasi-Static Positioning of Ionic Polymer – Metal Composite (IPMC) Actuators," *IEEE/ASME International Conference*, 24–28 July, Monterey, California, USA.